Supplementary Information: Energetics and chemistry at the electron selective interfaces for p-i-n perovskite solar cells: an in situ investigation

Karen Radetzky[a,b], Alberto García-Fernández[a,c], Birgit Kammlander[a], Evelyn Johannesson[a,b], Brian Rydgren[a,b], Rahul Mahavir Varma[a], Håkan Rensmo[a,b], and Ute B. Cappel[a,b]

[a] Division of X-ray Photon Science, Department of Physics and Astronomy, Uppsala University, Box 516, 751 20 Uppsala, Sweden

[b] Wallenberg Initiative Materials Science for Sustainability, Department of Physics and Astronomy, Uppsala University, 751 20 Uppsala, Sweden

[c] Interdisciplinary Center for Chemistry and Biology, Faculty of Science, University of A Coruña, 15071 A Coruña, Spain

1 Additional experimental details

1.1 Materials

Methylammonium iodide, lead iodide, bathocuproine, C_{60}, and γ - butyrolactone were purchased from Sigma Aldrich and used as received. Ag granules (Metalor) were used as a source in the thermal evaporation while the reference silver foil was purchased from Alfa Aesar.

1.2 Ag foil cleaning

The Ag foil was cleaned for 50 min by Ar^+ ion sputtering with an ion energy of 1 kV, $2 \cdot 10^{-6}$ mbar Ar-pressure, and 5 mA emission current.

2 Thickness calculations

The overlayer thickness d was calculated from the perovskite substrate peak decay. Within this approach, intermixing of the materials is neglected. As a further approximation the overlayer is assumed to be homogeneous and uniform. Moreover, the perovskite species is assumed to be evenly distributed within the substrate. The peak intensity of the relevant perovskite core level measured on the pristine surface is then given by Equation 1.

$$I_0 = K\sigma n \int_0^\infty e^{-\frac{z}{\lambda_1}} dz = K\sigma n\lambda_1 \tag{1}$$

Herein, K summarizes experimental and instrumental constants, σ denotes the elemental cross section of the probed substrate core level at the given photon energy, n represents the concentration of the investigated species in the probing volume, z is the depth in the sample, and λ_1 represents the inelastic mean free path

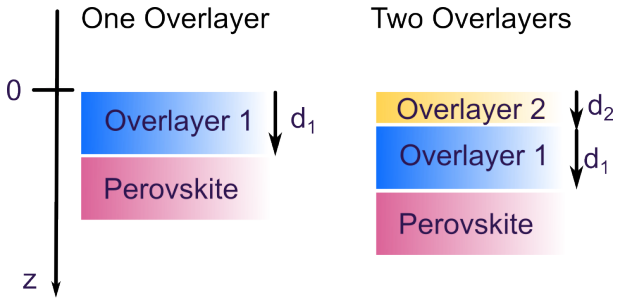

Figure S1: Illustration of the relevant sample architecture, thicknesses, and axis orientation for the above described calculations

(IMFP) of the photoelectron in the perovskite. After the deposition of an overlayer, the peak intensity can be described by Equation 2 instead.

$$I_{d_1} = K\sigma n e^{-\frac{d_1}{\lambda_2}} \int_{d_1}^{\infty} e^{-\frac{z-d_1}{\lambda_1}}\, dz = K\sigma n \lambda_1 e^{-\frac{d_1}{\lambda_2}} \tag{2}$$

The equation describes the generation of an photoelectron in the perovskite, the probability of collision-free travel to the interface, and subsequent escape through a material with a different IMFP λ_2. When relating this to the initial intensity of the core level peak, Equation 3 can be used to calculate the final thickness d_1 of the overlayer.

$$d_1 = ln(\frac{I_{d_1}}{I_0})(-\lambda_2) \tag{3}$$

When another layer with a different IMFP λ_3 and thickness is deposited on the already existing stack, this also needs to be considered when calculating the resulting substrate core level intensity (Equation 4).

$$I_{d_2} = K\sigma n e^{-\frac{d_1}{\lambda_2}} e^{-\frac{d_2}{\lambda_3}} \int_{d_1+d_2}^{\infty} e^{-\frac{z-d_1-d_2}{\lambda_1}}\, dz = K\sigma n e^{-\frac{d_1}{\lambda_2}} e^{-\frac{d_2}{\lambda_3}} \lambda_1 \tag{4}$$

Combining Equations 1,3, and 4, the thickness of the second overlayer d_2 can be calculated according to Equation 5.

$$d_2 = (ln(\frac{I_{d_2}}{I_0}) + \frac{d_1}{\lambda_2})(-\lambda_3) \tag{5}$$

Figure S1 illustrates the discussed sample architecture and relevant thicknesses.

For this experiment, the layer thicknesses were calculated based on the Pb 4f core level PE peak intensities. The IMFP of the Pb 4f photoelectron within the different materials was calculated based on the TPP-2M model (Table S1).[1,2] Table S2 summarizes the used values and resulting thicknesses.

Table S1: Parameters used and calculated IMFP employing the TPP-2M model.

Material	$E_{kin}(Pb\ 4f)$	ρ $[g/cm^3]$	Molar mass $[g/mol]$	Valence number	Band gap [eV]	λ $[nm]$
$MAPbI_3$	397	4.15	618.97	40	1.57	1.19
$MAPbI_3$	620	4.15	618.97	40	1.57	1.64
C_{60}	397	1.65	720.66	240	1.86	1.36
C_{60}	620	1.65	720.66	240	1.86	1.87
BCP	397	1.20	360.45	134	3.50	1.43
BCP	620	1.20	360.45	134	3.50	1.98

Additionally, the relative coverage γ of the overlayer of thickness d influences the decrease in intensity of a core level with IMFP λ (Equation 6).

$$I_d = I_0 * (1-\gamma) + \gamma * I_0 * e^{-\frac{d}{\lambda}} \tag{6}$$

Table S2: Summary of the input data for the thickness calculations presented in this work for both samples with a relatively thinner (1) and thicker (2) layer of BCP. Herein, I_0 corresponds to the Pb 4f core level intensity measured on the pristine perovskite, I_{d_1} after the evaporation of C_{60}, and I_{d_2} after the evaporation of BCP. The calculated thicknesses of the C_{60} and BCP layer are denoted as d_1 and d_2, respectively.

Sample	$h\nu[eV]$	I_0	I_{d_1}	I_{d_2}	$\lambda_1[nm]$	$\lambda_2[nm]$	λ_3 [nm]	d_1 [nm]	d_2 [nm]
1	535	6.68	0.37	0.17	1.19	1.35	1.43	3.9	1.1
1	758	1.32	0.14	0.07	1.64	1.87	1.98	4.1	1.5
2	535	4.12	1.17	0.03	1.19	1.35	1.43	1.7	5.3
2	758	1.95	0.64	0.02	1.64	1.87	1.98	2.1	6.6

2.1 Calculation to estimate BCP complex distribution

The N 1s spectrum acquired with 535 eV after the deposition of silver onto the second model system with 6 nm of BCP indicates the formation of a complex with BCP and silver. Due to high overlap of the N 1s region with the Ag MNN Auger feature in measurements with 758 eV incident photon energy, the depth distribution of the complex cannot be assessed via comparison between measurements with two photon energies. Instead, we have used the relative intensity of the new feature to the main peak to gain insight. We model the system as two separate layers to determine if the BCP complex could form a continuous layer on top of a layer of BCP in which the molecules are not complexed. For this, we assume a finite layer of thickness d_c at the top of the sample in which all BCP molecules are in a complex. Moreover, the adjacent BCP layer contains no molecules that act as ligands and has an infinite depth compared to the probing depth of the experiment. We neglect modifications to the IMFP λ_c of the N 1s photoelectron due to the complexation and any effect from the covering silver layer (this assumes that the covering silver effects both layers in the same way). Except for the kinetic energy of the escaping photoelectron, the parameters for calculating λ_c in a BCP layer can be found in Table S1. We also assume the concentration n of nitrogen to be equal in both layers. The intensity from the top layer I_c can be calculated with Equation 7 and the intensity from the lower layer I_B is described by Equation 2 when using λ_c.

$$I_c = K\sigma n \int_0^{d_c} e^{-\frac{z}{\lambda_c}} dz \tag{7}$$

Equation 8 then gives the thickness of the layer that only contains the complex.

$$d_c = ln(\frac{I_c}{I_B} + 1)\lambda_c \tag{8}$$

Using the values from Table S3, this gives a calculated thickness of 0.1 nm. This value is not feasible for describing a separate layer as it is below the dimensions of the molecule. This indicates that either only a smaller fraction of the BCP molecule at the surface are converted to the BCP complex or that there is no separate layer in the interfacial region that solely contains the complex. In the latter case, the complex molecules are instead mixed within the BCP layer. Assuming a uniform distribution, 16% of the BCP molecules would be in a complex based on the intensities of the two N 1s peaks.

Table S3: Summary of the input data for the thickness calculations for an assumed interfacial layer of a silver complex with BCP. Herein, I_B corresponds to the N 1s core level intensity of the main peak in the N 1s PE spectrum after the final deposition of silver onto the second model system, while I_c is the intensity of the new N 1s feature in the same spectrum. The calculated thickness of the assumed overlayer is given as d_c.

Sample	$h\nu[eV]$	I_B	I_c	$E_{kin}(N\ 1s)$	$\lambda_c\ [nm]$	$d_c\ [nm]$
$MAPbI_3/C_{60}$/BCP(6 nm)/Ag	535	3.26	0.62	135	0.74	0.1

3 Additional PE spectra

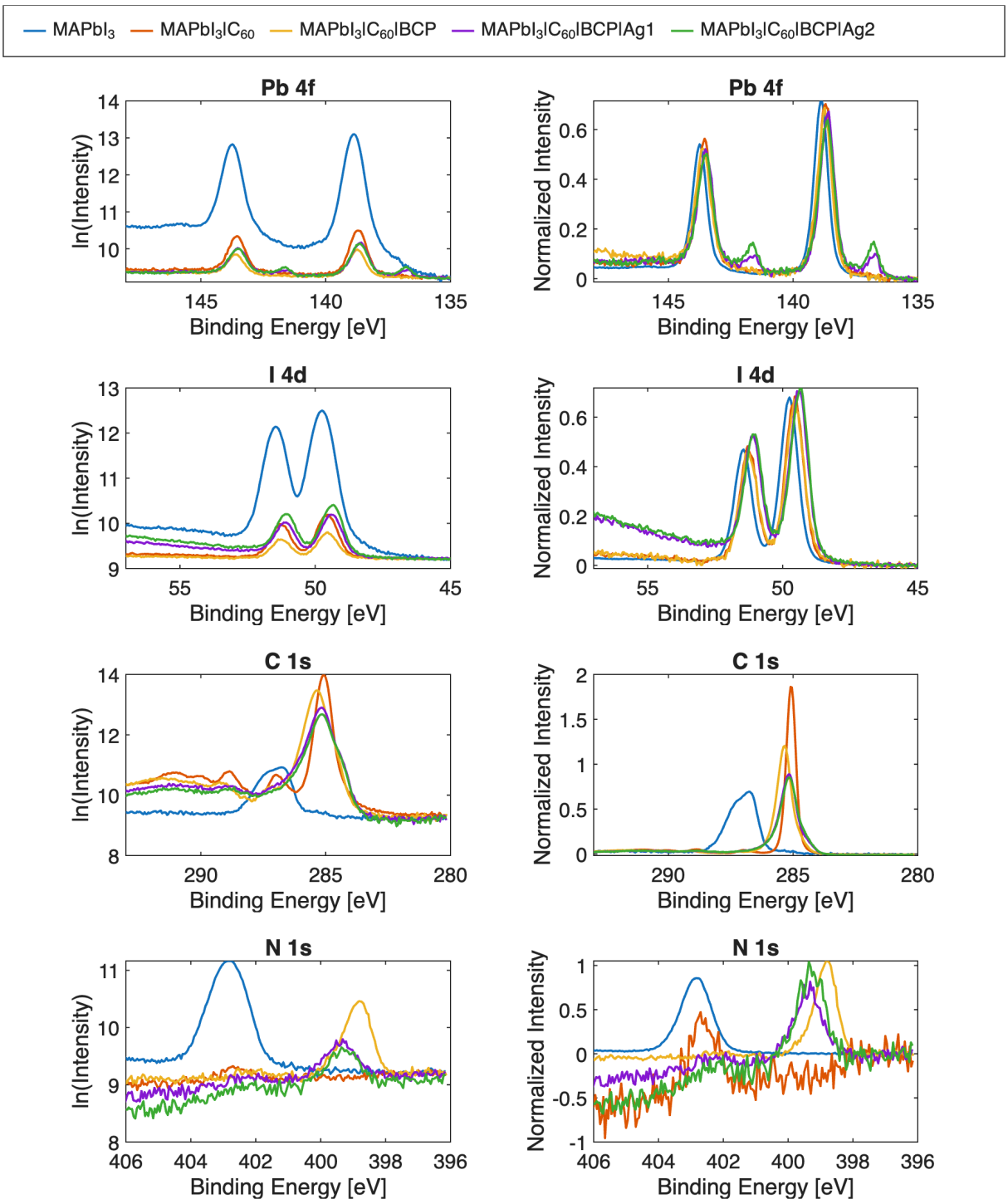

Figure S2: PE spectra recorded with 535 eV incident photon energy after the evaporation of additional layers onto crystal 1, energy referenced to the Fermi level ($E_b(Au\ 4f_{7/2}) = 84.0\ eV$). The left column shows the binding energy versus the natural logarithm of the measured intensity. The spectra were aligned to the background. The right column shows the spectra intensity normalized to the main peak.

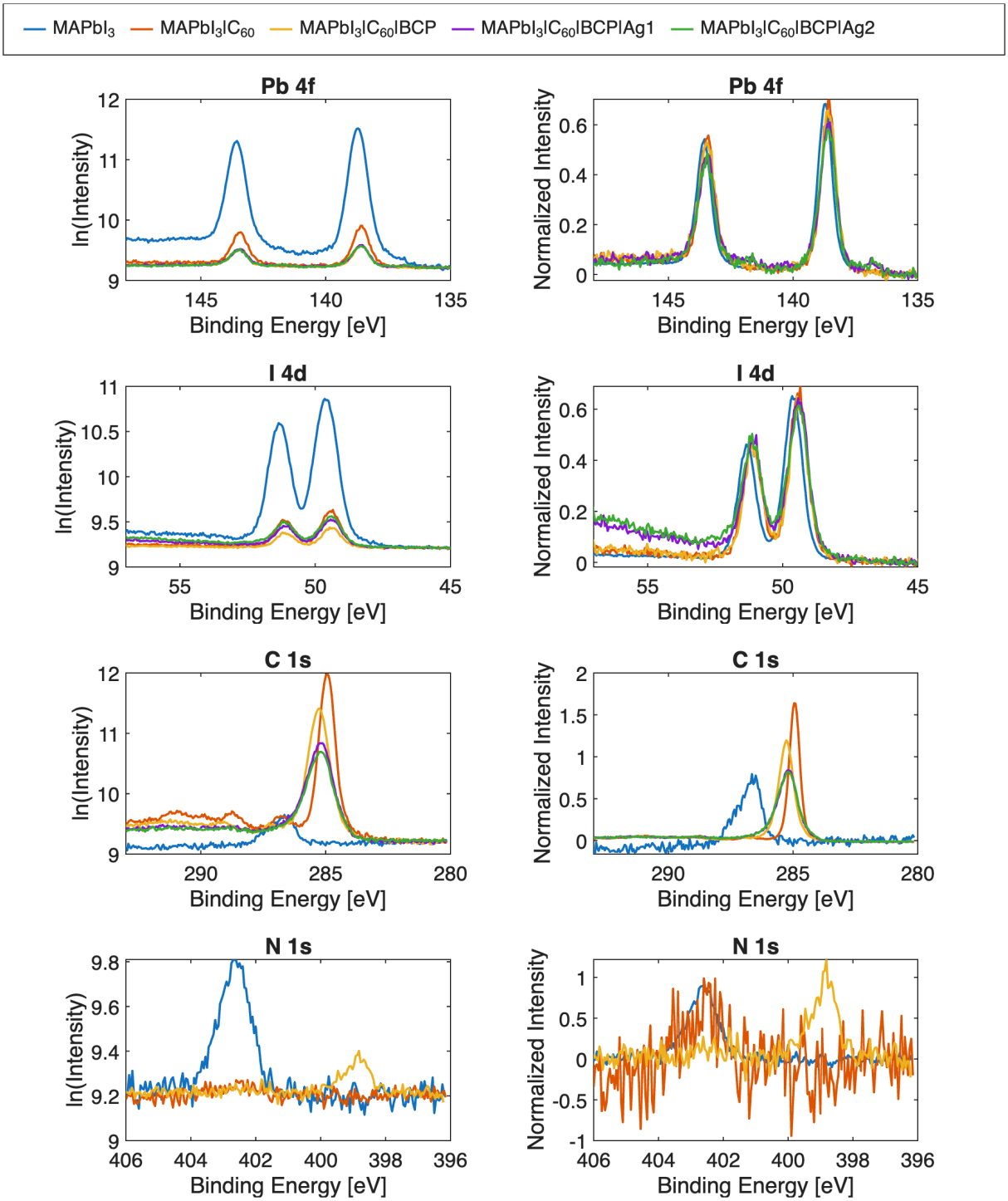

Figure S3: PE spectra recorded with 758 eV incident photon energy after the evaporation of additional layers onto crystal 1, energy referenced to the Fermi level ($E_b(Au\ 4f_{7/2}) = 84.0\ eV$). The left column shows the binding energy versus the natural logarithm of the measured intensity. The spectra were aligned to the background. The right column shows the spectra intensity normalized to the main peak. The N 1s spectra are omitted after the evaporation of silver due to high overlap with the Ag MNN feature.

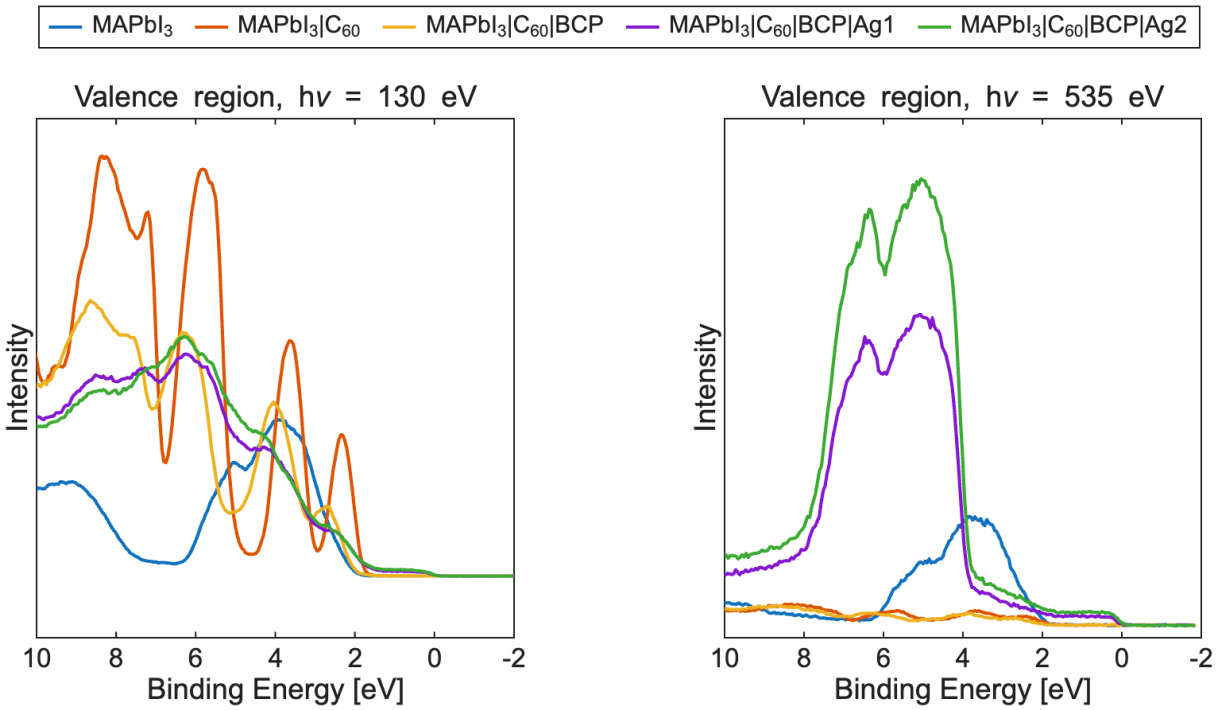

Figure S4: Valence region PE spectra recorded with 130 eV (left) and 535 eV (right) incident photon energy after the evaporation of additional layers onto crystal 1, energy referenced to the Fermi level ($E_b(Au\ Fermi\ edge) = 0.0\ eV$).

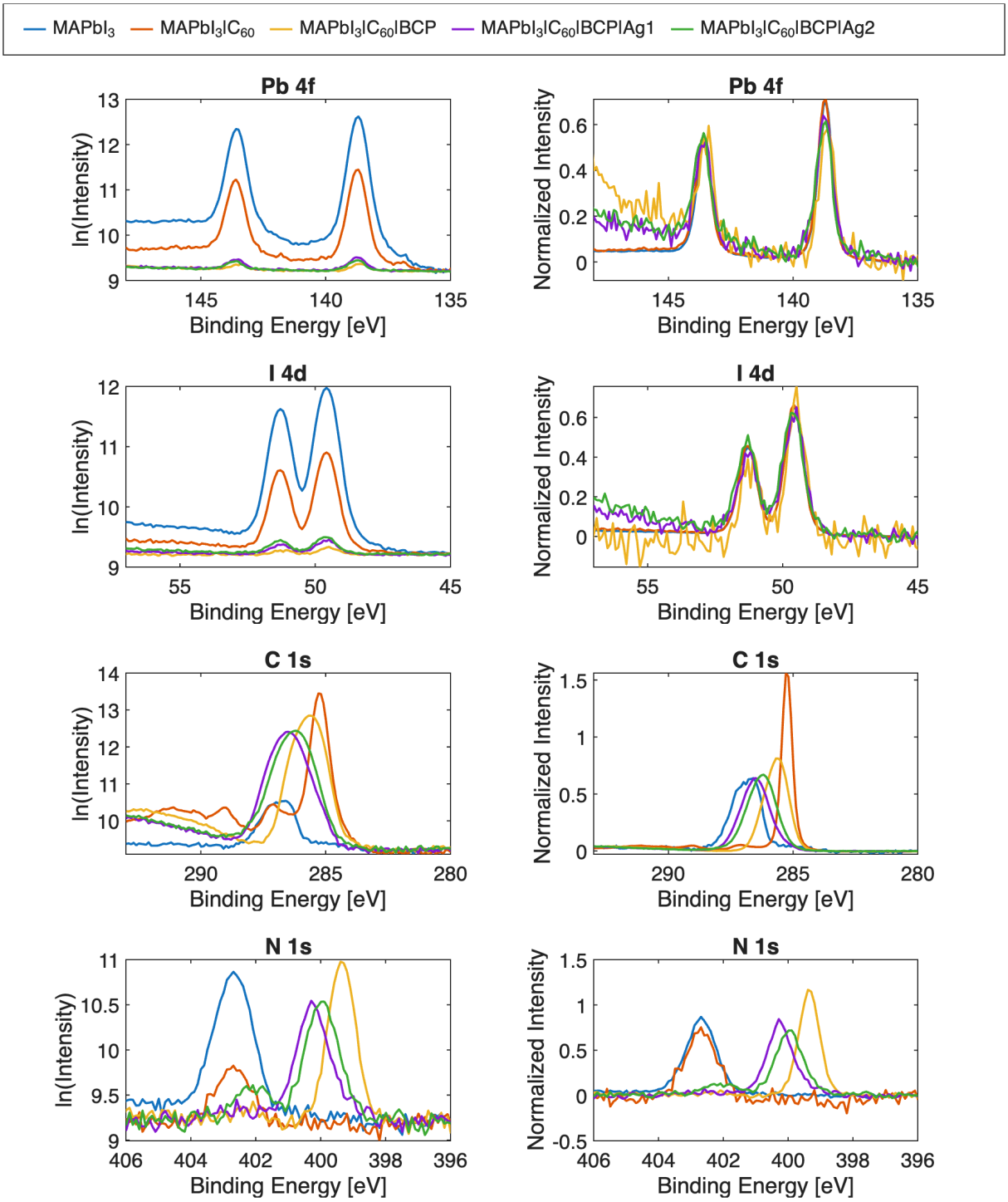

Figure S5: PE spectra recorded with 535 eV incident photon energy after the evaporation of additional layers onto crystal 2, energy referenced to the Fermi level ($E_b(Au\ 4f_{7/2}) = 84.0\ eV$). The left column shows the binding energy versus the natural logarithm of the measured intensity. The spectra were aligned to the background. The right column shows the spectra intensity normalized to the main peak.

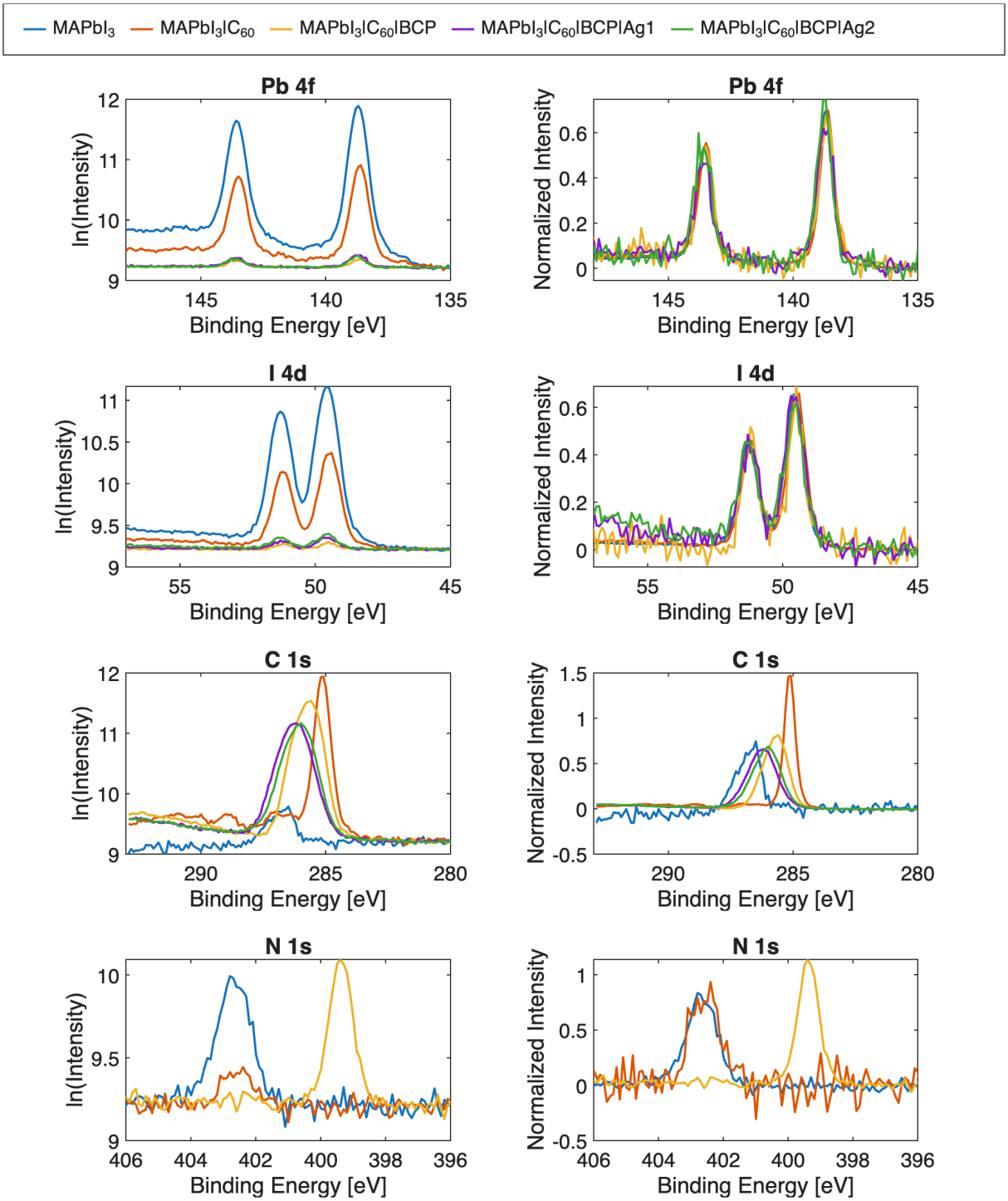

Figure S6: PE spectra recorded with 758 eV incident photon energy after the evaporation of additional layers onto crystal 2, energy referenced to the Fermi level ($E_b(Au\ 4f_{7/2}) = 84.0\ eV$). The left column shows the binding energy versus the natural logarithm of the measured intensity. The spectra were aligned to the background. The right column shows the spectra intensity normalized to the main peak. The N 1s spectra are omitted after the evaporation of silver due to high overlap with the Ag MNN feature.

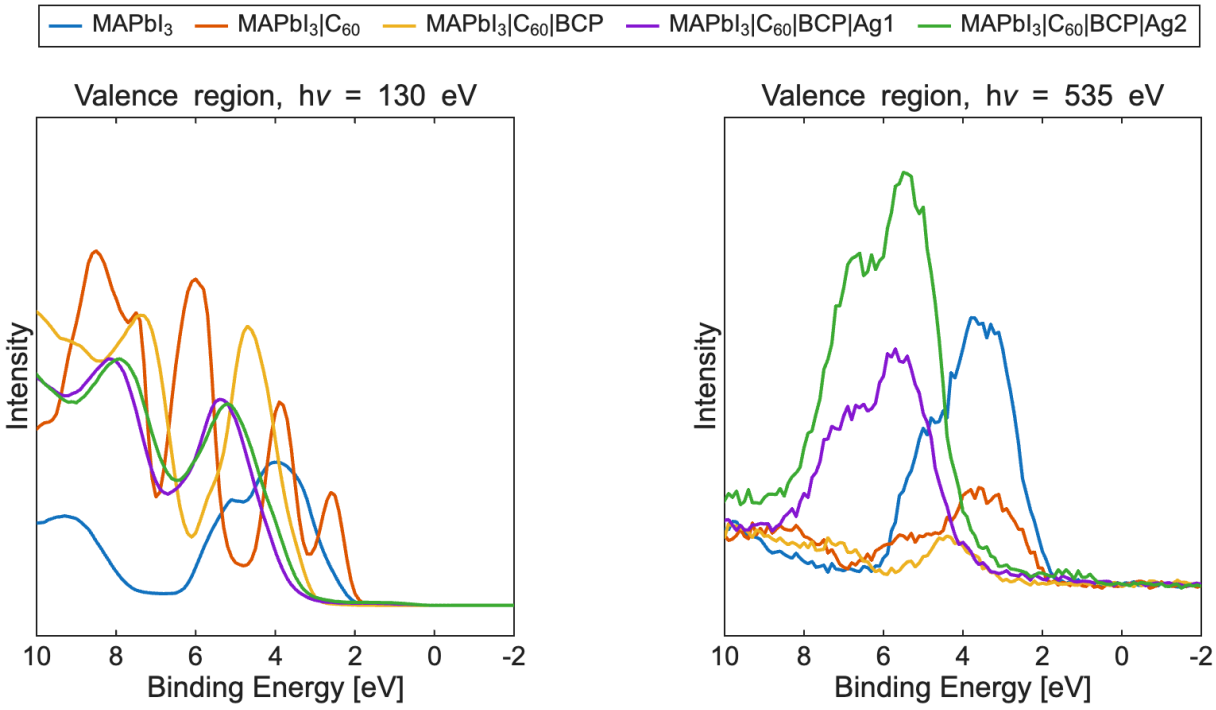

Figure S7: Valence region PE spectra recorded with 130 eV (left) and 535 eV (right) incident photon energy after the evaporation of additional layers onto crystal 2, energy referenced to the Fermi level ($E_b(Au\ Fermi\ edge) = 0.0\ eV$).

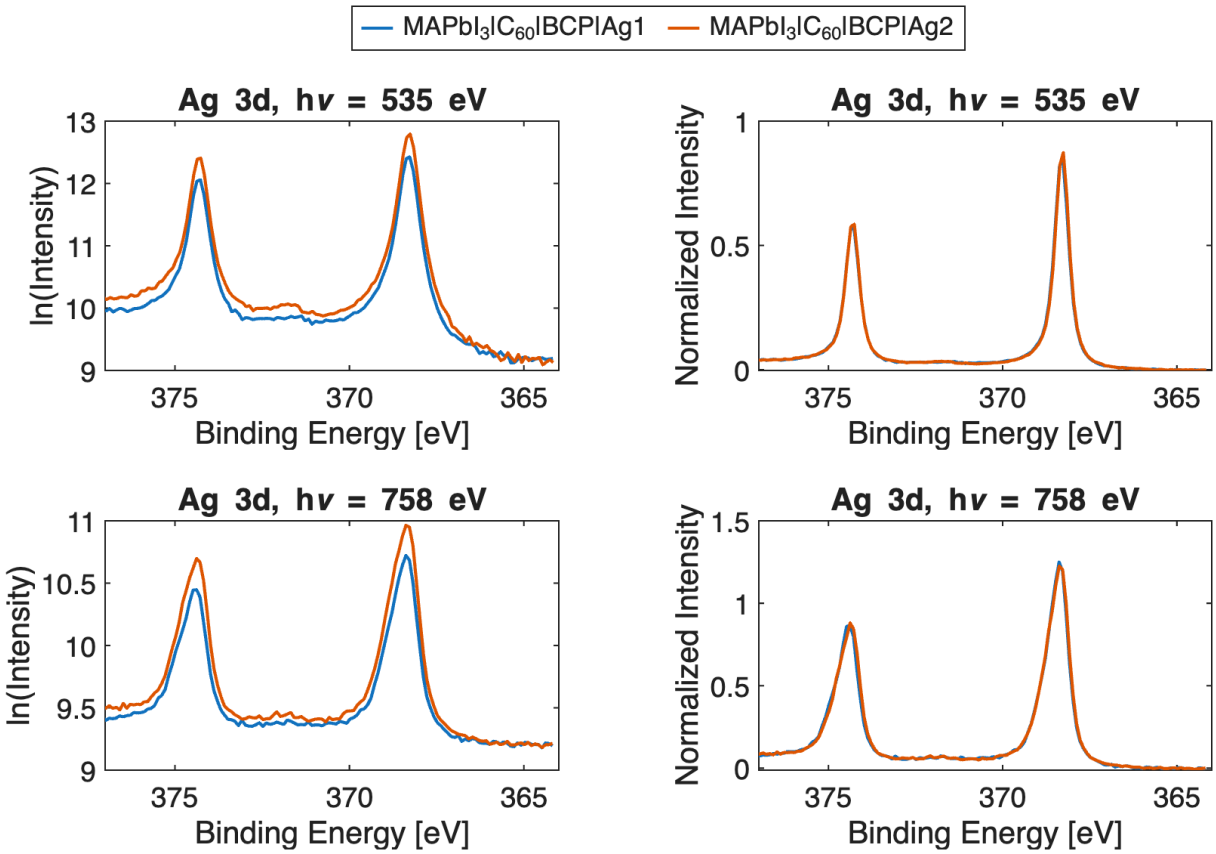

Figure S8: Ag 3d PE spectra recorded with 535 eV (top) and 758 eV (bottom) incident photon energy after the evaporation of additional layers onto crystal 1, energy referenced to the Fermi level ($E_b(Au\ 4f_{7/2}) = 84.0\ eV$). The left column shows the binding energy versus the natural logarithm of the measured intensity. The spectra were aligned to the background. The right column shows the spectra intensity normalized to the main peak.

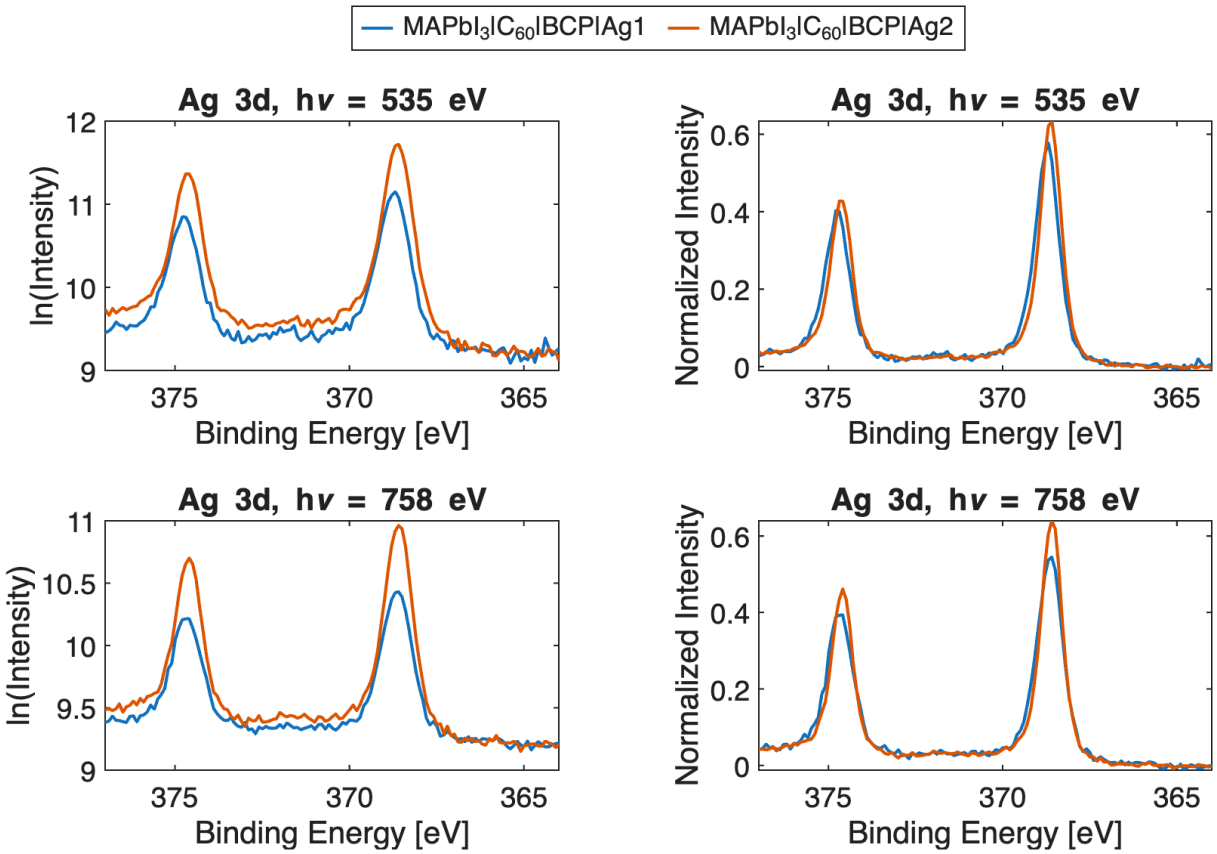

Figure S9: Ag 3d PE spectra recorded with 535 eV (top) and 758 eV (bottom) incident photon energy after the evaporation of additional layers onto crystal 2, energy referenced to the Fermi level ($E_b(Au\ 4f_{7/2}) = 84.0\ eV$). The left column shows the binding energy versus the natural logarithm of the measured intensity. The spectra were aligned to the background. The right column shows the spectra intensity normalized to the main peak.

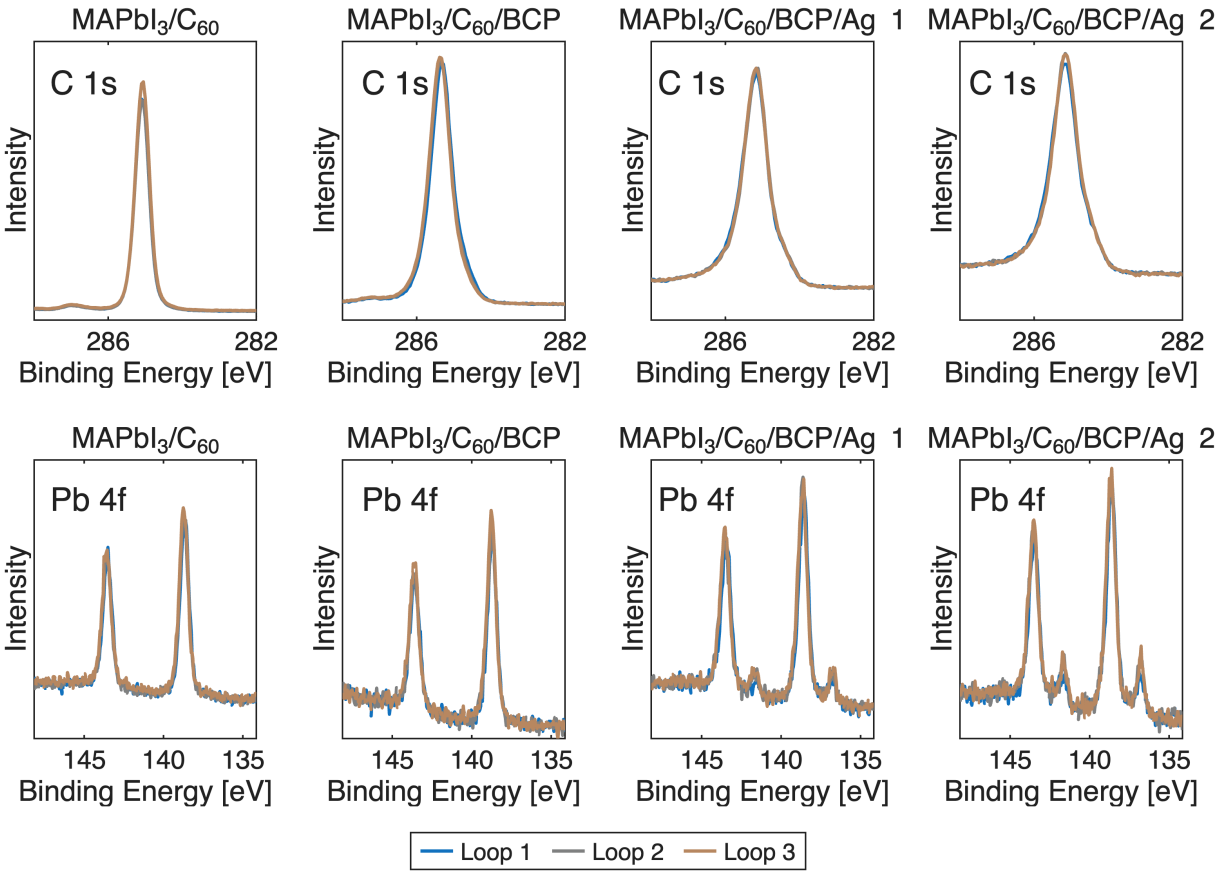

Figure S10: C 1s and Pb 4f PE spectra recorded with 535 eV incident photon energy. All individual measurements of the looped sequence are shown for all sample architectures involving the organic charge transport layers. The time between each loop iteration for a specific core level is approximately 20 min. The spectra are energy referenced to the Fermi level ($E_b(Au\ 4f_{7/2}) = 84.0\ eV$).

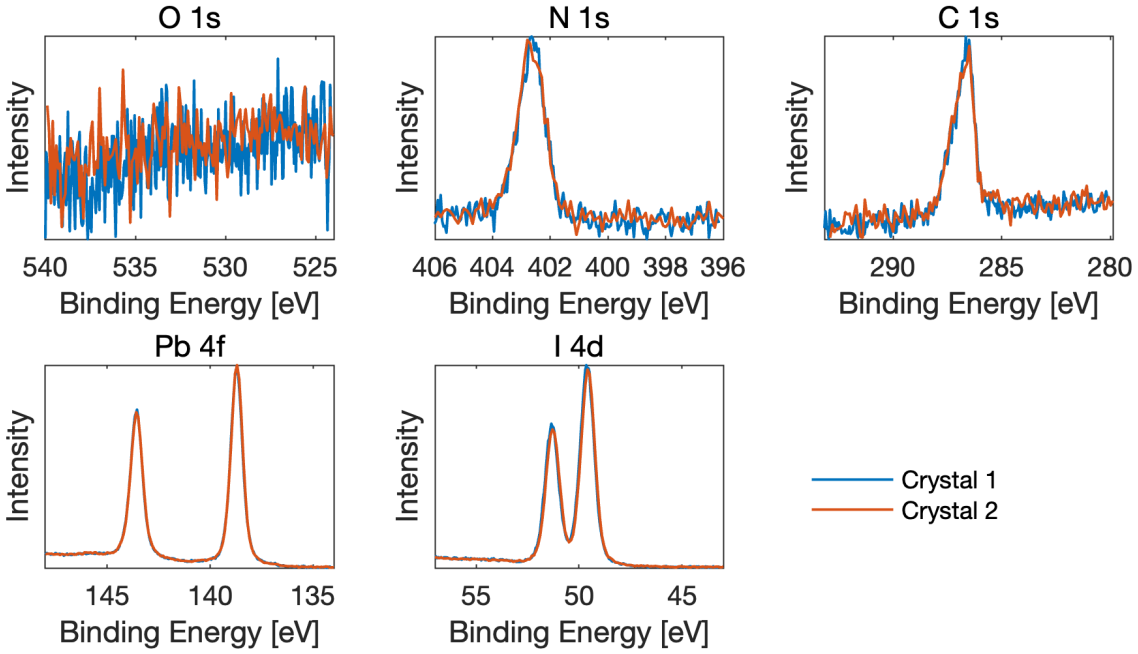

Figure S11: The shown core level spectra are recorded at 758 eV incident X-ray energy, energy referenced to the Fermi level ($E_b(Au\ 4f_{7/2}) = 84.0\ eV$), and intensity normalized to the respective Pb 4f peak. All core level peaks can be fully attributed to $MAPbI_3$. There is no indication of surface contamination.

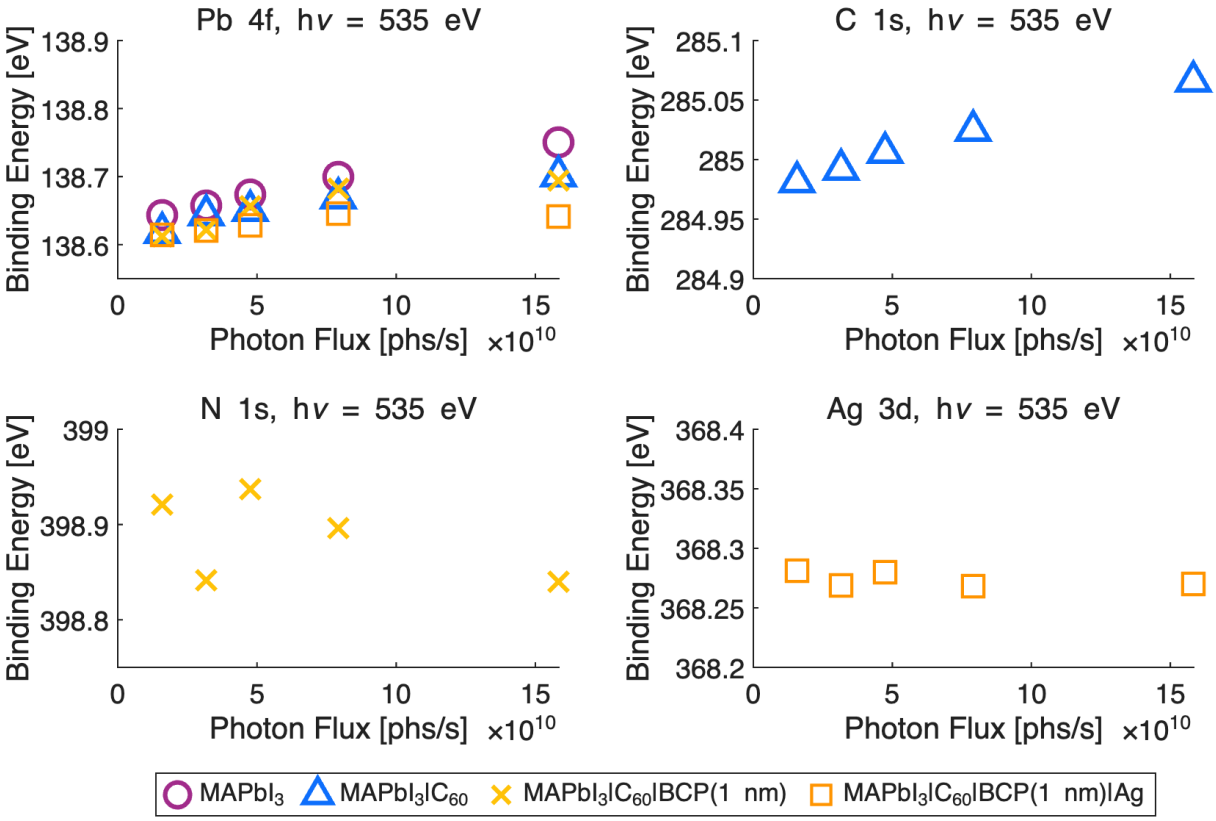

Figure S12: The measured and Fermi level calibrated ($E_b(Au\ 4f_{7/2}) = 84.0\ eV$) binding energy of the Pb 4f, C 1s, N 1s, or Ag 3d core level peak is shown as a function of incident photon flux for the consecutive assembly stages. The measurements reveal minor sample charging of less than 0.1 eV for until the evaporation of BCP. After the evaporation of BCP, sample charging becomes negligible and the peak positions are considered stable.

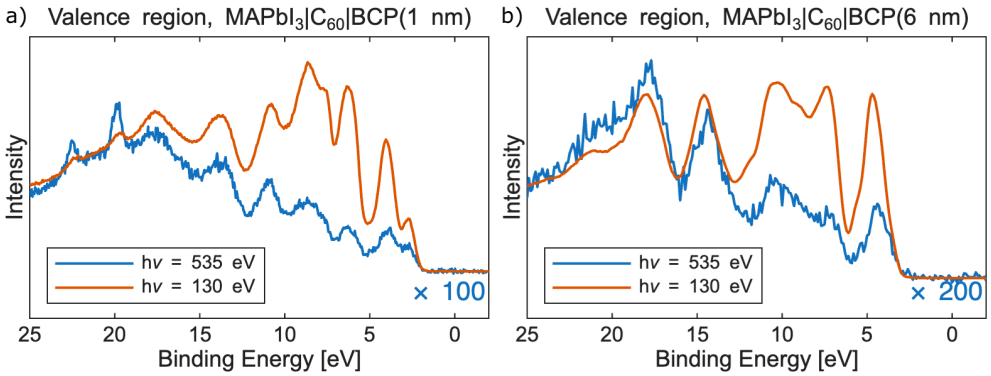

Figure S13: Valence region spectra recorded on a) $MAPbI_3/C_{60}/BCP(1\ nm)$ and b) $MAPbI_3/C_{60}/BCP(6\ nm)$ with 535 eV (blue) and 130 eV (red) incident photon energy. While the valence band measurements at 130 eV and 535 eV overlap fully for the first model system, an energetic difference of - 0.18 eV is present between the different photon energies for the BCP reference. Therefore, the valence spectrum of the BCP reference is energy calibrated so that the N 1s core level peak position recorded with 535 eV aligns with the N 1s core level peak position measured on the primary model system with an additional shift of - 0.18 eV in the main manuscript.

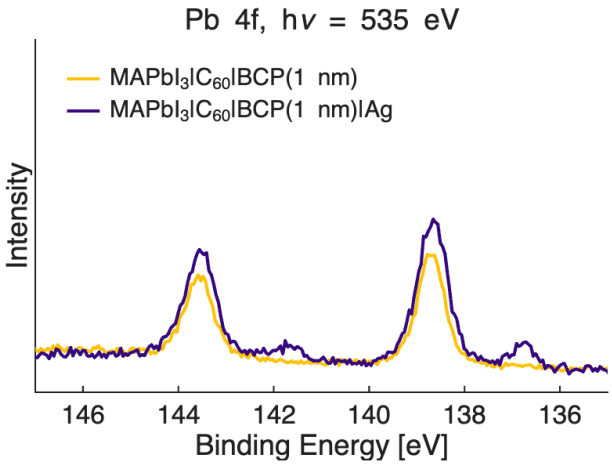

Figure S14: Pb 4f PE spectra acquired in a secondary measurement spot with lower X-ray exposure at a photon energy of 535 eV, energy calibrated to the Fermi level ($E_b(Au\ 4f_{7/2}) = 84.0\ eV$). A feature attributed to metallic lead emerges after the evaporation of silver.

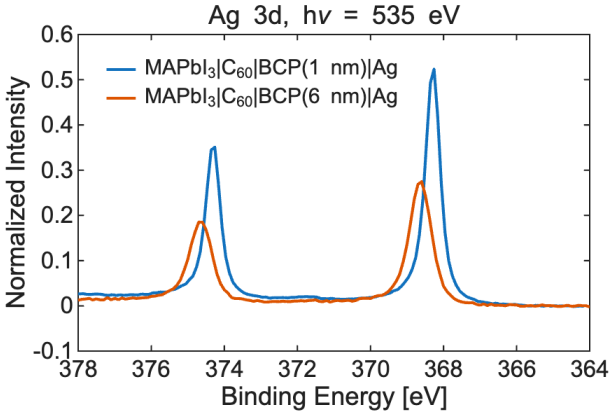

Figure S15: Ag 3d PE spectra measured on a $MAPbI_3/C_{60}$/BCP(1 nm)/Ag model half cell (blue) and a $MAPbI_3/C_{60}$/BCP(6 nm)/Ag model half cell (red) acquired at 535 eV normalized to the intensity of the Pb 4f core level peak of the respective pristine crystal and calibrated to the Fermi level ($E_b(Au\ 4f_{7/2}) = 84.0\ eV$).

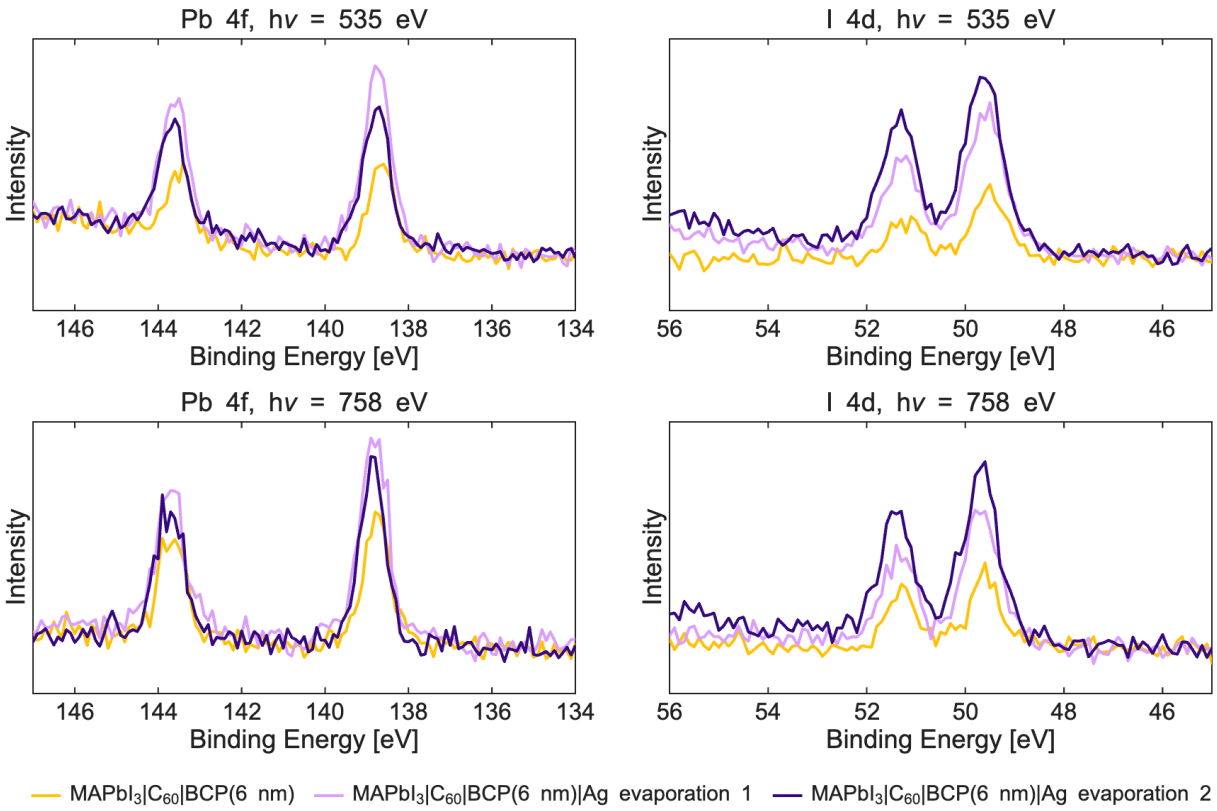

Figure S16: Pb 4f and I 4d PE spectra acquired at 535 eV and 758 eV before (yellow) and after (purple) consecutive evaporations of silver on $MAPbI_3/C_{60}/BCP(6\ nm)$, calibrated to the Fermi level ($E_b(Au\ 4f_{7/2}) = 84.0\ eV$).

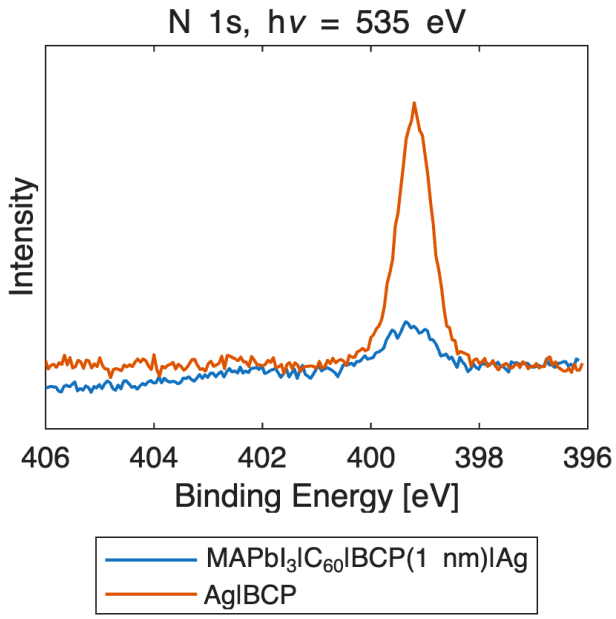

Figure S17: N 1s spectra acquired with 535 eV incident photon energy on a $MAPbI_3/C_{60}/BCP(1\ nm)/Ag$ model half cell (blue) and BCP evaporated on silver foil (red).

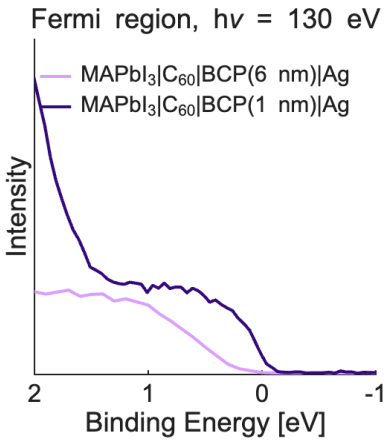

Figure S18: Fermi region measured with 130 eV incident photon energy on $MAPbI_3/C_{60}$/BCP(1 nm)/Ag (dark purple) and $MAPbI_3/C_{60}$/BCP(6 nm)/Ag (light purple).

4 Comparison to $Cs_xFA_{1-x}PbI_3$

In this section, we present additional data on a cleaved $Cs_xFA_{1-x}PbI_3$ (FA = formamidinium) single crystal substrate, which was investigated during the same evaporation steps as model system 2 for $MAPbI_3$ presented in the main article. This data is used to determine how the observed iodide and Pb^{2+} ion migration and chemical reactions between silver and BCP for the second model system depend on perovskite composition. While we were able to fabricate an equivalent of the second model system on a mixed cation $Cs_xFA_{1-x}PbI_3$ single crystal substrate during the beamtime, the signal-to-noise ratio is lower for high overlayer thicknesses and some beam-induced damage cannot be fully excluded in late measurements of the main measurement spot. Additionally, due to limited experimental time and sample availability, we did not reproduce the first model system with a thin BCP layer on a $Cs_xFA_{1-x}PbI_3$ single crystal. We include the full obtained data set here to present the gathered data set in its context and provide a reference for future investigations.

The $Cs_xFA_{1-x}PbI_3$ single crystal was synthesized via inverse temperature crystallization from equimolar amounts of FAI and PbI_2 dissolved in GBL to make a 1 M solution. 4 mol% of CsI were added. The precursors were dissolved at 50 °C and single crystals were formed and removed at 110 °C. The cleaved single crystal was characterized via PES. The produced surface does not have any additional contamination and all peaks could be attributed to the perovskite (Figure S19). CsI was added in the synthesis to ensure the formation of a black perovskite phase and the inclusion of a small amount of Cs^+ in the crystal structure is confirmed by the detection of a Cs 4d signal at the cleaved sample surfaces (Figure S19).

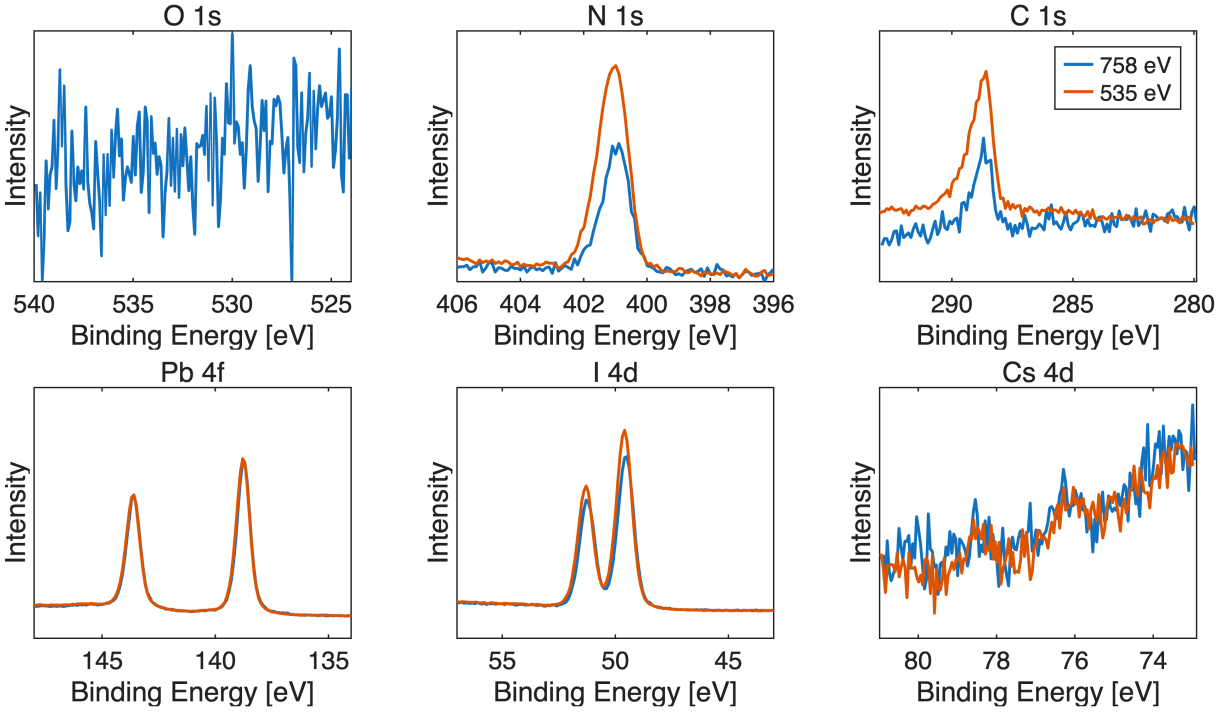

Figure S19: Core level spectra recorded on a cleaved surface of a $Cs_xFA_{1-x}PbI_3$ crystal at 758 eV (blue) and 535 eV (red) incident X-ray energy, energy calibrated to the Fermi level ($E_b(Au\ 4f_{7/2}) = 84.0\ eV$), and intensity normalized to the intensity of the respective Pb 4f peak. All core level peaks can be fully attributed to $Cs_xFA_{1-x}PbI_3$. There is no indication of surface contamination.

The full $Cs_xFA_{1-x}PbI_3$-based model system was prepared alongside the second $MAPbI_3$ model system. The layer thickness calculations are fairly consistent: There is very good agreement when comparing values based on the Pb 4f and the I 4d core level peak attenuation but measurements with 535 eV incident photon energy give lower values than calculations based on measurements with 758 eV. The results are presented in Table S4. As the $Cs_xFA_{1-x}PbI_3$ single crystal was mounted next to the $MAPbI_3$ single crystal for all

depositions, we assume that the final thickness of all transport layers should be comparable between the two different systems. The full set of characterization spectra from all steps of the in situ fabrication is shown in Figure S20 - S22.

Table S4: Summary of the input data for the thickness calculations for $Cs_xFA_{1-x}PbI_3$. Herein, I_0 corresponds to the core level intensity measured on the pristine perovskite, I_{d_1} after the evaporation of C_{60}, and I_{d_2} after the evaporation of BCP. The calculated thicknesses of the C_{60} and BCP layer are denoted as d_1 and d_2, respectively.

Core level	$h\nu[eV]$	I_0	I_{d_1}	I_{d_2}	$\lambda_1[nm]$	$\lambda_2[nm]$	λ_3 [nm]	d_1 [nm]	d_2 [nm]
Pb 4f	535	421.6	58.9	0.6	1.21	1.35	1.43	2.7	6.5
Pb 4f	758	195.3	31.8	0.7	1.66	1.87	1.98	2.9	8.0
I 4d	535	210.5	31.8	0.6	1.39	1.56	1.65	3.0	6.7
I 4d	758	84.3	19.2	0.4	1.84	2.07	2.20	3.1	8.3

In the fully assembled model system, the signal-to-noise ratio for the residual perovskite peaks is low and inhibits straightforward data interpretation. In the following, we therefore discuss some qualitative observations do not present a quantitative analysis of the changes. As observed for the $MAPbI_3$-based model system, the measured I 4d PE peak intensity increases after each deposition of silver (Figure S23). This demonstrates that the iodide ions are mobile and can permeate the assembled charge transport layers also in the case of a $Cs_xFA_{1-x}PbI_3$ perovskite. The intensity of the Pb 4f PE peaks only increases for measurements with 758 eV incident photon energy. In both, the spectra acquired with 535 eV and with 758 eV photon energy, there might be an additional smaller feature at lower binding energy of the Pb $4f_{7/2}$ related to metallic lead after the final deposition of silver. However, this could just be due to the high noise level and sloped background shape. A corresponding feature at lower binding energy of the Pb $4f_{5/2}$ is not clearly discernible in measurements with either photon energy and therefore the presence of metallic lead is not confirmed.

Figure S24 shows the Pb 4f PE spectra measured in a control spot with lower X-ray exposure before and after each evaporation of silver. The peak intensity trend is different from the observations made in the main spot. First of all, there is a clear increase in the Pb 4f PE peak intensity after the deposition of silver indicating the migration of Pb^{2+} towards the surface. Secondly, there is no additional feature at higher binding energies of the Pb $4f_{7/2}$. As the signal-to-noise ratio is better in the control spot and the X-ray exposure is lower compared to the main spot, the absence of metallic lead is the more reliable result and consistent with our observations on the second $MAPbI_3$-based model system.

Figure S24 additionally shows the N 1s spectra recorded in the main measurement spot and the control spot on the $Cs_xFA_{1-x}PbI_3$-based model system after the evaporation of silver. For both measurement spots, a distinct feature at 402.1 eV binding energy is present. As for the $MAPbI_3$ and gold substrate model systems, we propose that this relates to the complexation of Ag by BCP. The Ag MNN Auger peak indicates an oxidation state of +I (FigureS24). Additionally, the N 1s spectrum in the main measurement spot contains a smaller feature at lower binding energy compared to the main BCP peak. As this is not reproduced in the control spot, it is very likely that this is a product of beam damage, potentially of the formamidinium cation.

In summary, we observe ion migration and silver complexation for a model system based on a second perovskite composition, namely $Cs_xFA_{1-x}PbI_3$. The results are in good agreement with our presented study on $MAPbI_3$-based model systems and therefore indicate that the same processes can happen upon interface formation in formamidnium iodide-based as in methylammnoium iodide-based lead halide perovskites. A

quantitative analysis of the processes in $Cs_xFA_{1-x}PbI_3$ requires further experiments.

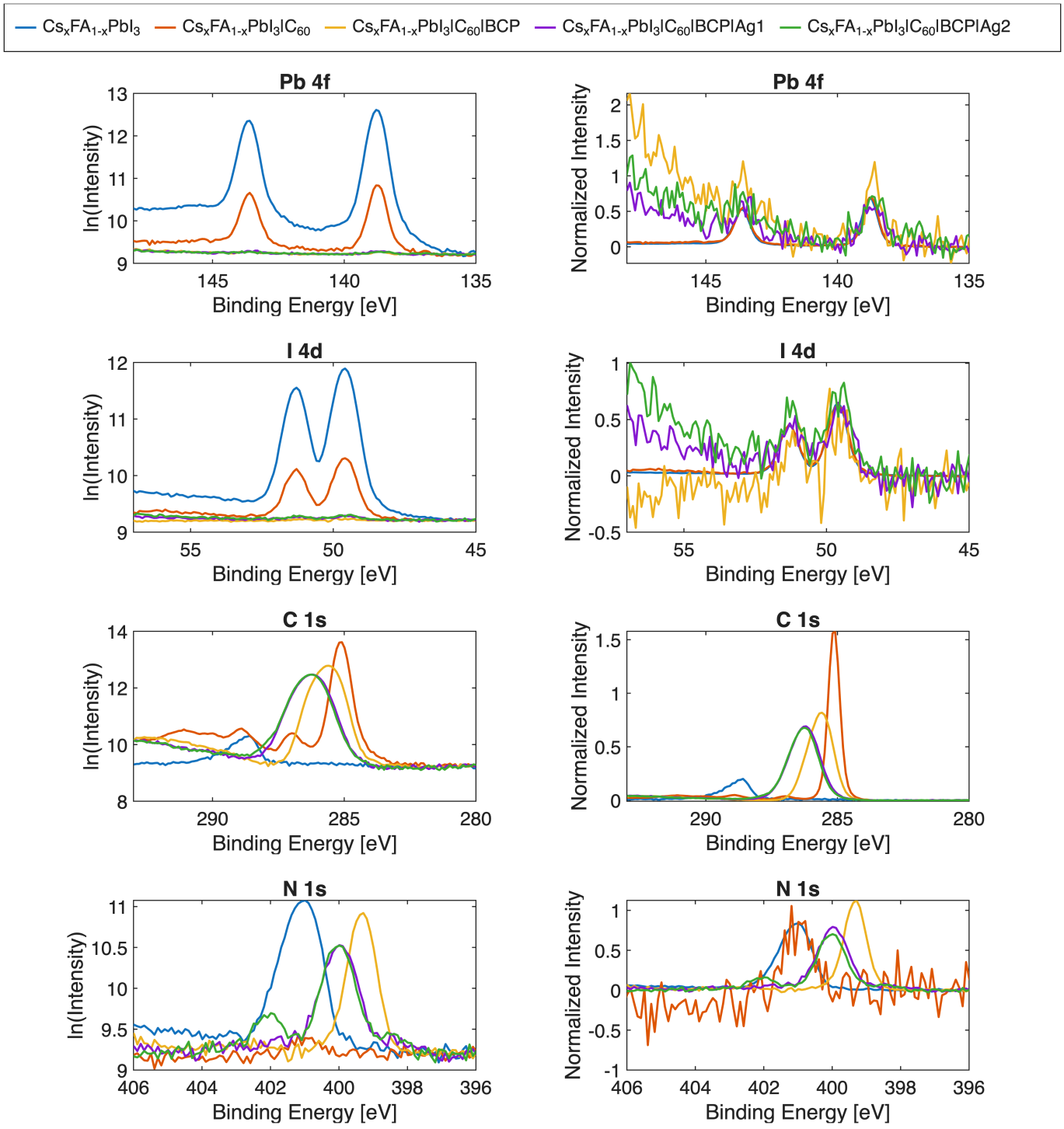

Figure S20: PE spectra recorded with 535 eV incident photon energy after the evaporation of additional layers onto $Cs_xFA_{1-x}PbI_3$, energy referenced to the Fermi level ($E_b(Au\ 4f_{7/2}) = 84.0\ eV$). The left column shows the binding energy versus the natural logarithm of the measured intensity. The spectra were aligned to the background. The right column shows the spectra with the intensity normalized to the main peak.

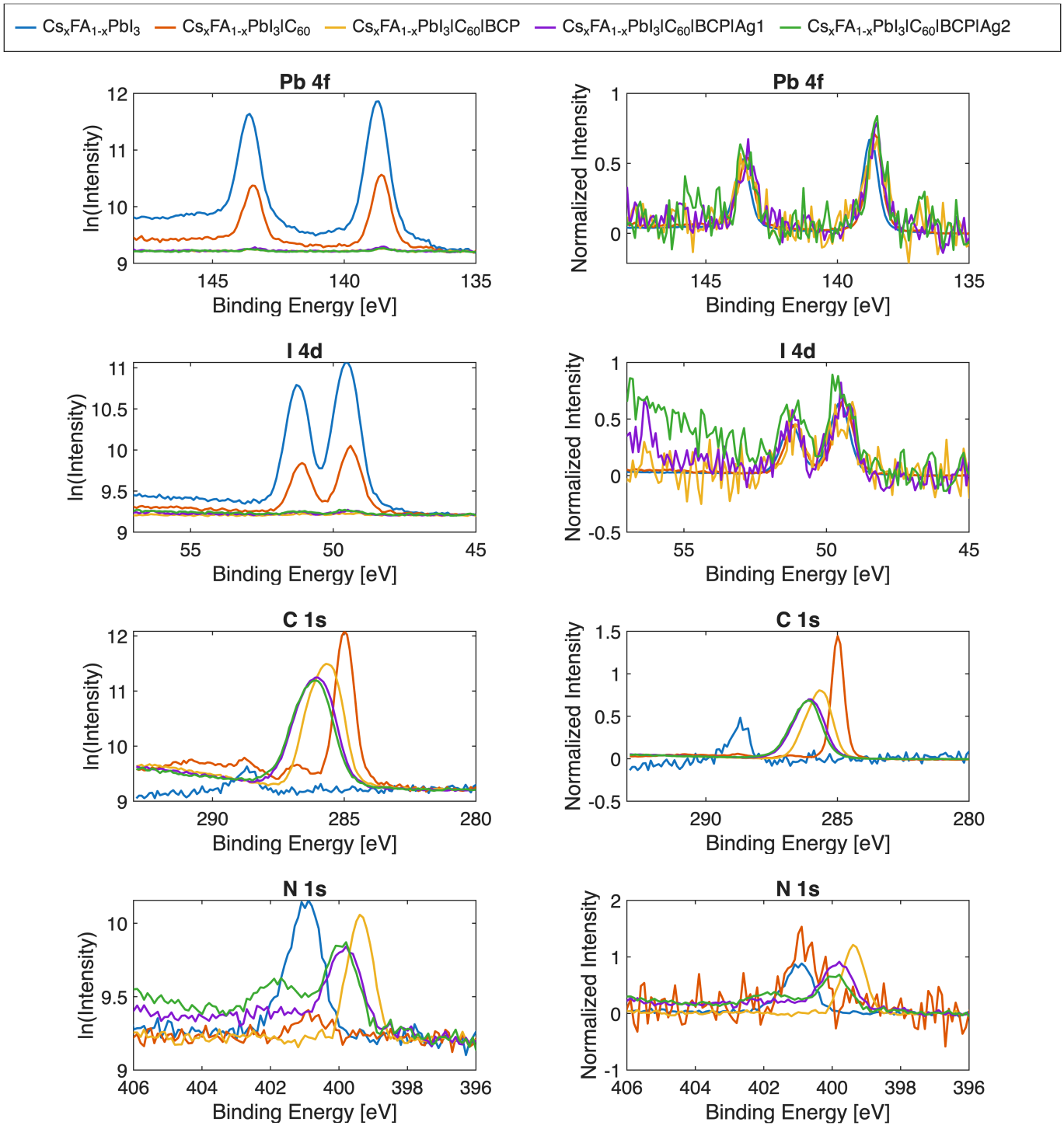

Figure S21: PE spectra recorded with 758 eV incident photon energy after the evaporation of additional layers onto $Cs_xFA_{1-x}PbI_3$, energy referenced to the Fermi level ($E_b(Au\ 4f_{7/2}) = 84.0\ eV$). The left column shows the binding energy versus the natural logarithm of the measured intensity. The spectra were aligned to the background. The right column shows the spectra with the intensity normalized to the main peak.

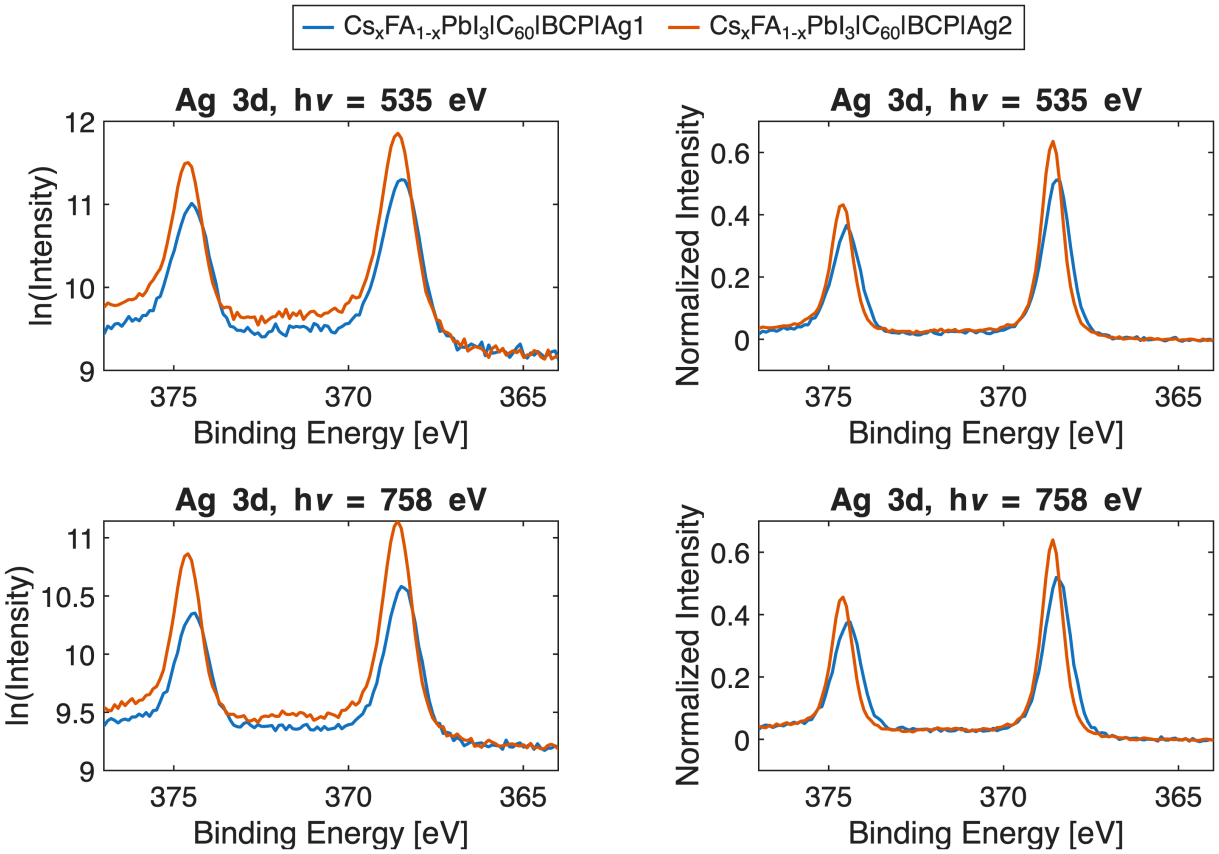

Figure S22: PE Ag 3d core level spectra recorded with 535 eV (top) and 758 eV (bottom) incident photon energy on $Cs_xFA_{1-x}PbI_3$, energy referenced to the Fermi level ($E_b(Au\ 4f_{7/2}) = 84.0\ eV$). The left column shows the binding energy versus the natural logarithm of the measured intensity. The spectra were aligned to the background. The right column shows the spectra intensity normalized to the main peak.

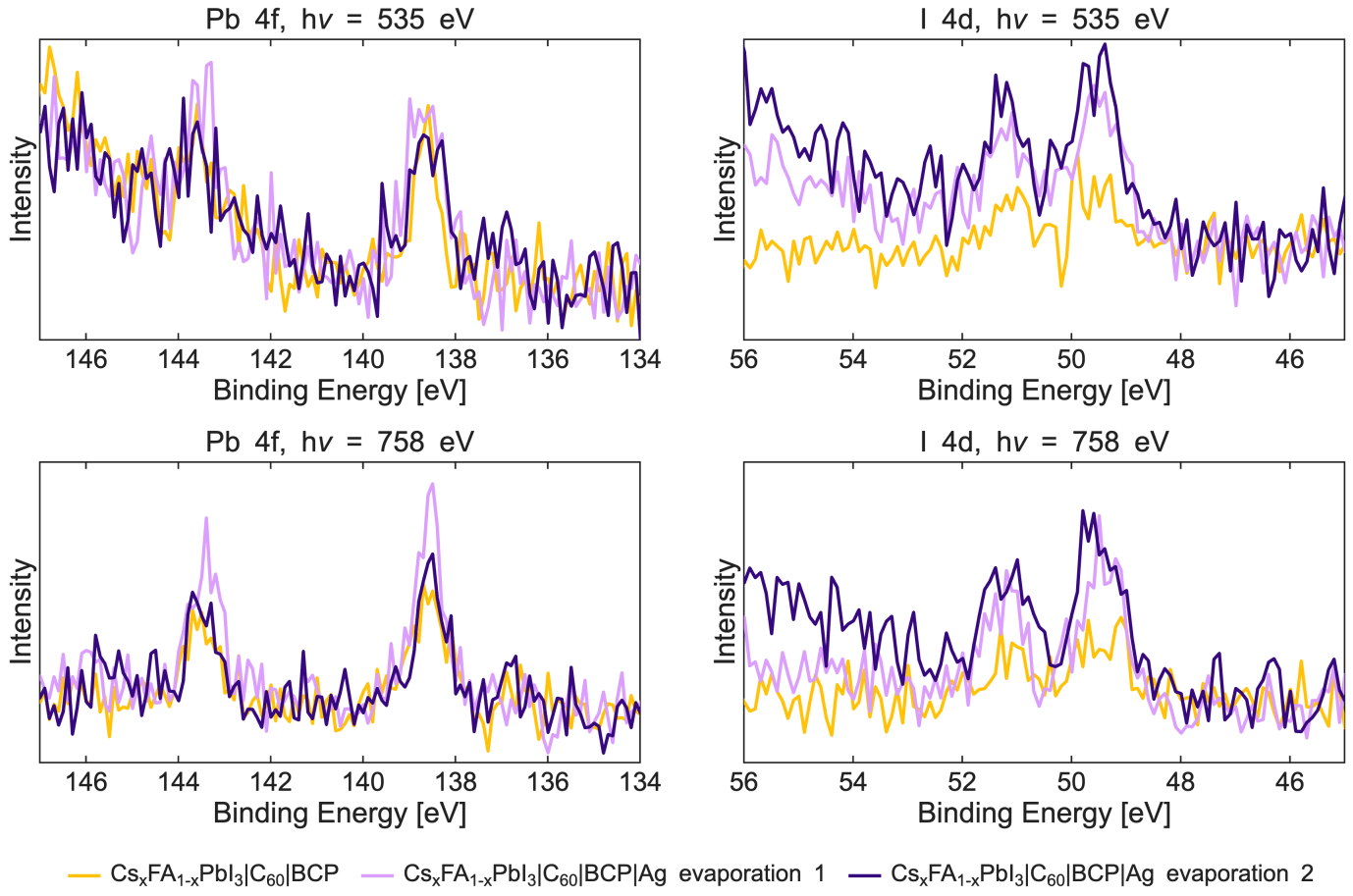

Figure S23: Pb 4f and I 4d PE spectra acquired at 535 eV and 758 eV before (yellow) and after (purple) consecutive evaporations of silver on $Cs_xFA_{1-x}PbI_3/C_{60}$/BCP, calibrated to the Fermi level (Au $4f_{7/2}$ = 84.0 eV).

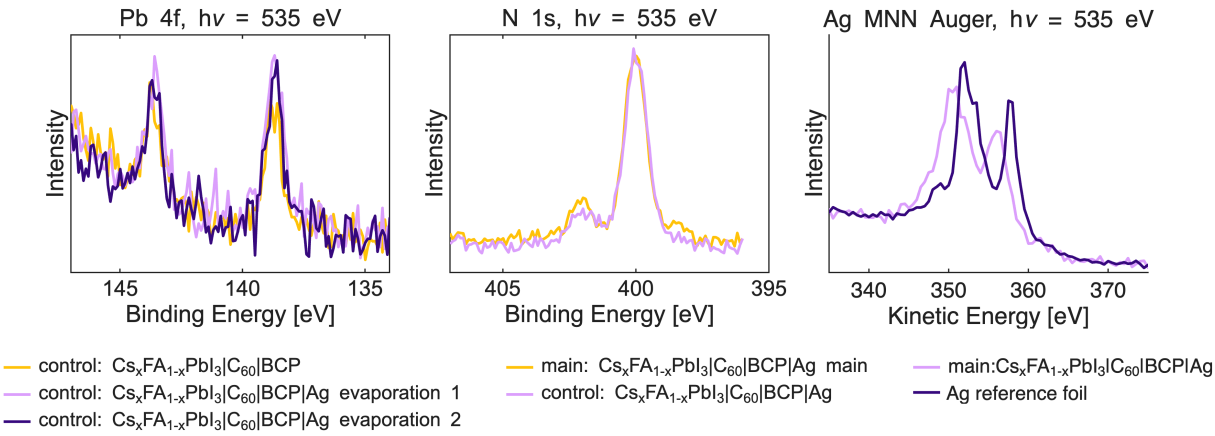

Figure S24: Pb 4f PE spectra recorded in the control spot on with an incident photon energy of 535 eV before (yellow) and after (purple) consecutive depositions of silver on $Cs_xFA_{1-x}PbI_3/C_{60}$/BCP (left). N 1s PE spectra recorded in the main and control spot on with an incident photon energy of 535 eV after the deposition of silver on $Cs_xFA_{1-x}PbI_3/C_{60}$/BCP (middle). All spectra are calibrated to the Fermi level ($E_b(Au\ 4f_{7/2})$ = 84.0 eV). Ag MNN spectra on $Cs_xFA_{1-x}PbI_3/C_{60}$/BCP/Ag and a silver reference foil (right).

References

(1) Tanuma, S.; Powell, C. J.; Penn, D. R. *Surface and interface analysis* **1994**, *21*, 165–176.
(2) Tanuma, S.; Powell, C. J.; Penn, D. R. *Surface and interface analysis* **2003**, *35*, 268–275.